PURIFICATION STRATEGIES AND BIOLOGICAL EVALUATION OF PHENYLPROPANOIDS FROM LONICERA MACRANTHOIDES HAND-MAZZ

Danli Peng^{1#}, Lei Qiao^{1#}, Wei Yan², Lang Xue¹, Shenggang Yang³, Jiaqi Yu⁴, Nanping Zhang¹, Juxiang Kuang¹, Gang Wang¹ and Guanghua Yan²*

School of Pharmacy, Zunyi Medical University, Zunyi, Guizhou 563000, China

Keywords: Macroporous Resin, Total Phenylpropanoids, Purification, Molecular Docking, Bioactivity, Lonicera macranthoides extract

Abstract

Phenylpropanoids, a class of bioactive compounds found in *Lonicera macranthoides* Hand.-Mazz, are known for their diverse pharmacological properties. This study focused on the purification of total phenylpropanoids (TP) from *Lonicera macranthoides* extract (LME) using nine types of macroporous resins. Among them, HPD-100 resin exhibited the highest purification efficiency. Optimal conditions for purification were determined as follows: extract concentration of 10 mg/ml, solution pH of 3, resin dosage of 7 g, elution solution concentration of 60%, elution volume of 30 ml, loading rate of 1.5 ml/min, loading volume of 200 ml, elution rate of 2.0 ml/min, and elution volume of 220 ml. Adsorption kinetics conformed to the pseudo-second-order model, while thermodynamic analysis aligned with the Freundlich isotherm model, indicating spontaneous and exothermic adsorption with negative values for enthalpy, entropy, and Gibbs free energy. Molecular docking further revealed π - π and π - σ interactions between the resin and phenylpropanoid molecules, with a docking score of -3.388 kcal/mol, supporting the resin's affinity for the target compounds. These findings provide a robust foundation for the efficient extraction and functional evaluation of phenylpropanoids from *L. macranthoides*.

Introduction

Lonicera macranthoides Hand.-Mazz (Caprifoliaceae) is a perennial evergreen climber or shrub mainly distributed in southwest China. Its dried flower buds or early blooms serve as a medicinal source of Lonicerae Flos (Liu et al. 2013). It demonstrates remarkable antioxidant, antibacterial, anti-inflammatory, and immunomodulatory activities (He et al. 2019), which are primarily attributed to its diverse array of secondary metabolites, including phenylpropanoids, triterpenoid saponins, and iridoids (Liu et al. 2024). Among these, phenylpropanoids (C6-C3) are known to exert strong antioxidant, anti-inflammatory, and antimicrobial effects, making them valuable bioactive compounds in both pharmaceutical and nutraceutical applications. The major phenylpropanoid constituents of L. macranthoides include chlorogenic acid (CA), isochlorogenic acid A (IAA), isochlorogenic acid C (IAC), and neochlorogenic acid (NA) (Li et al. 2022). However, their extraction and purification from complex plant matrices remain challenging due to low content and interference from coexisting compounds. To address this, macroporous adsorption resins (MARs) have been widely applied for the selective enrichment and purification of phenolic compounds owing to their high adsorption capacity, reusability, and mild operating conditions. Therefore, this study systematically evaluated nine types of MARs to determine the optimal resin for phenylpropanoid purification from L. macranthoides, optimized both static and dynamic adsorption/desorption parameters, and analyzed adsorption kinetics, isotherms, thermodynamics to elucidate the mechanism of phenylpropanoid-resin interactions.

^{*}Author for correspondence: <wg8855350@zmu.edu.cn>. ¹School of Pharmacy, Zunyi Medical University, Zunyi, Guizhou 563000, China. ²Guizhou Miaolao Biological Health Co. Ltd. Zunyi, Guizhou 563000, China. ³Jibang Changsheng Honeysuckle Agricultural Technology Co. Ltd. Suining County, Zunyi, Guizhou 563000, China. ⁴Third Affiliated Hospital of the Zunyi Medical University, Zunyi, Guizhou 563000, China. *Contributed equally to the article.

Materials and Methods

Dried *Lonicera macranthoides* was procured from Suiyang Lonicera Flos Industry Co. Ltd. (Zunyi, China). Both HPLC-grade methanol and HPLC-grade acetonitrile were obtained from Anhui Zesheng Technology Co. Ltd. (Anhui, China). NA, CA, IAC and IAA were obtained from Chengdu Refined Biological Technology Co. Ltd. (Chengdu, China). Macroporous resins S-8, AB-8, NKA-9, DM130, HPD450, D101, HPD100, SP825 and HPD600 were all obtained from Shanghai Yuanye Bio-Technology Co. Ltd. (Shanghai, China).

TP content was quantified following a modified version of the method reported by (Liu *et al.* 2024), using HPLC-UV (320 nm) with a Phenomenex C18 column and gradient elution. LME was prepared following a modified version of the method reported by (Liu *et al.* 2024), involving ultrasonic-assisted extraction with 60% methanol, vacuum concentration, and vacuum drying. Macroporous resins were pretreated following a modified version of the described method (Li *et al.* 2018).

A precisely measured amount of macroporous resin was weighed and mixed with 25 ml of LME solution. To optimize the static adsorption conditions, the effects of various factors, including mass concentration (2.5-12.5 mg/ml), pH (2-6), resin dosage (1-9 g), eluent concentration (20-100%), and eluent volume (20-40 ml), were systematically investigated. Adsorption and desorption properties were calculated using the corresponding formulas. For each experiment, 1.0 g of every macroporous resin was accurately weighed and transferred into separate conical flasks. Then, 25 ml of LME solution (5 mg/ml) was added to each flask. The flasks were tightly sealed and incubated in a thermostatic oscillator at 37°C with a shaking speed of 150 rpm for 24 hrs. After incubation, the mixtures were vacuum-filtered to separate and collect the resins for further analysis. Adsorption properties were determined based on the equations below:

Adsorption ratio (A, %) =
$$[(C_0 \times V_1 - C_e \times V_2)/C_0 \times V_1] \times 100$$

Adsorption capacity (qe, mg/g) = $[(C_0 \times V_1 - C_e \times V_2)]/W$

Resin desorption was performed in 25 ml of anhydrous methanol with agitation under identical conditions for an additional 24 hrs. The mixture was then vacuum-filtered to isolate the resins. The desorption properties were calculated using the following equations:

$$\begin{split} \text{Desorption ration (D, \%)} &= (C_d \times V_d) \, / [(C_0 \times V_1 - C_e \times V_2)] \times 100 \\ &\quad \text{Desorption capacity (qd, mg/g)} &= (C_d \times V_d) / W \end{split}$$

In this equation, C_0 , C_e , and Cd_d (mg.ml⁻¹) refer to TP concentrations in the initial, equilibrium, and desorption media, respectively; V_1 , V_2 , and V_d (ml) indicate the volumes of sample, equilibrium solution, and eluate; and W (g) is the weight of the pretreated macroporous resin.

A specified volume of macroporous resin was packed into a chromatographic column, with the bed volume (BV) set at 20 ml (1 BV). The column was rinsed with deionized water until the effluent became clear and alcohol-free. A constant-flow pump controlled the sample loading rate (1.5-2.5 ml/min). After sample loading, the column was washed with deionized water to remove residual interstitial liquid, followed by elution at the same flow rate (1.5-2.5 ml/min) regulated by the pump. During the adsorption and desorption processes, the effluent was collected in 20 ml fractions, resulting in a total of 15 fractions. The total phenylpropanoid (TP) content in each fraction was determined by HPLC, and concentrations were calculated accordingly.

For the adsorption kinetics experiment, 7.0 g of macroporous resin was mixed with 25 ml of LME solution (10.0 mg/ml, pH 3) in a 50 ml conical flask. The flask was placed in a thermostatic

oscillator at 37°C and 150 rpm. At specified time intervals (10, 20, 30, 40, 50, 60, 80, 100, 120, 180, 240, 300, 360, 420, and 480 min), aliquots were collected and immediately replenished with an equal volume of blank solvent. The TP content in each sample was quantified, and adsorption kinetics were analyzed by monitoring the change in adsorption capacity over time. Adsorption behavior was further described by fitting the data to pseudo-first-order, pseudo-second-order, and intraparticle diffusion models according to the following equations: $\ln(q_e - q_t) = -k_1 t + \ln qe$; $t/q_t = 1/(k_2q_e^2) + t/q_e$; and $qt = k_p t^{1/2} + C$. Here, q_t (mg/g) represents the adsorption capacity at time t (min); k_1 (min⁻¹), k_2 (g·mg⁻¹·min⁻¹), and k_p (mg·g⁻¹·min^{-1/2}) are the kinetic constants for the pseudo-first-order, pseudo-second-order, and intraparticle diffusion models, respectively; and C (mg/g) denotes the boundary layer thickness constant.

For the adsorption isotherm experiments, 7.0 g of macroporous resin was added to 25 ml of LME solution (pH 3) at mass concentrations of 2.5, 5, 7.5, 10, and 12.5 mg/ml. The mixtures were incubated in a thermostatic oscillator at 150 rpm for 2 hrs at 25°C, 35°C, and 45°C. After incubation, the mixtures were vacuum-filtered to separate the resin, and the TP content in the filtrate was determined. The adsorption data were fitted to the Langmuir, Freundlich, and Temkin isotherm models described by the equations $C_e/q_e = 1/(K_LQ_m) + C_e/Q_m$, $\ln q_e = (1/n) \ln C_e + \ln K_F$, and $q_e = B_T \ln K_T + B_T \ln C_e$, respectively. In these models, Q_m (mg/g) denotes the maximum adsorption capacity, K_L (ml/mg), K_F [(mg/g)(ml/mg)^{1/n}], and K_T (ml/mg) are the equilibrium constants, 1/n reflects the adsorption intensity, and B_T (J/mol) represents the Temkin constant associated with adsorption heat.

For thermodynamic studies, 25 ml of LME solution (pH 3) at different concentrations was introduced into conical flasks containing 7.0 g of the selected macroporous resin. The flasks were shaken at 150 rpm for 2 h at 25°C, 35°C, and 45°C, then vacuum-filtered, and TP concentrations were determined by HPLC. Thermodynamic parameters were calculated using the equations $\ln K = -\Delta H/(RT) + \Delta S/R$ and $\Delta G = -RT \ln K$, where T (K) is the absolute temperature, R is the universal gas constant, and K is the equilibrium constant. The Freundlich exponent n indicates adsorption heterogeneity, while ΔH (enthalpy, kJ/mol), ΔG (Gibbs free energy, kJ/mol), and ΔS (entropy, kJ/mol) describe the thermodynamic nature of adsorption.

To elucidate the adsorption mechanism at the molecular level, chlorogenic acid (CA), a primary phenylpropanoid in *Lonicera macranthoides* with strong antioxidant and antibacterial activity, was subjected to molecular docking with the macroporous resin. The 3D structure of CA was constructed from its 2D PubChem model using AutoDock Tools 1.5.7. Docking simulations were performed with AutoDock Vina 1.2.5 using a grid spacing of 0.375 Å and an exhaustiveness value of 8. Both CA and the resin polymer were treated as flexible ligands, and the highest-affinity binding conformation was analyzed to explore possible adsorption interactions.

All experimental data were expressed as mean \pm standard deviation (SD). Statistical differences among groups were evaluated using one-way analysis of variance (ANOVA), with statistical significance set at p < 0.05.

Result and Discussion

Adsorption-desorption of TP on nine macroporous resins varied with resin polarity, surface area, and pore size (Alizadeh *et al.* 2024). Resin SP825 showed the highest adsorption but poor desorption, whereas HPD600 had the best desorption but lower adsorption; AB-8 and HPD100 performed similarly (Fig. 1). Polar phenylpropanoids favored adsorption on more polar resins (Hou *et al.* 2021). Balancing performance and cost, HPD100 was chosen for further study.

The pH of the sample solution exerts a marked effect on macroporous resin adsorption performance. The phenylpropanoid compounds in *Lonicera macranthoides* are

polyhydroxyphenolic acids (Dai *et al.* 2024), which predominantly exist in their molecular form under acidic conditions. This molecular state enhances their affinity for macroporous resins, thereby promoting a higher adsorption capacity (Wang *et al.* 2023). As pH increased from 2 to 3, the adsorption ratio of resin HPD100 steadily rose; beyond pH 3, its adsorption performance dropped abruptly. Optimal adsorption performance was observed at pH 3, with statistically distinct values compared to all other tested pH conditions (Fig. 2A). When the pH exceeds 3, the carboxyl and hydroxyl groups within the molecule progressively undergo deprotonation, existing in their ionic form (Sun *et al.* 2015). As a result, these compounds exhibit a reduced affinity for adsorption onto the resin. Given that the adsorption capacities showed no significant differences between pH 2.0 and 3.0, pH 3.0 was selected as the optimal pH value for the sample solution.

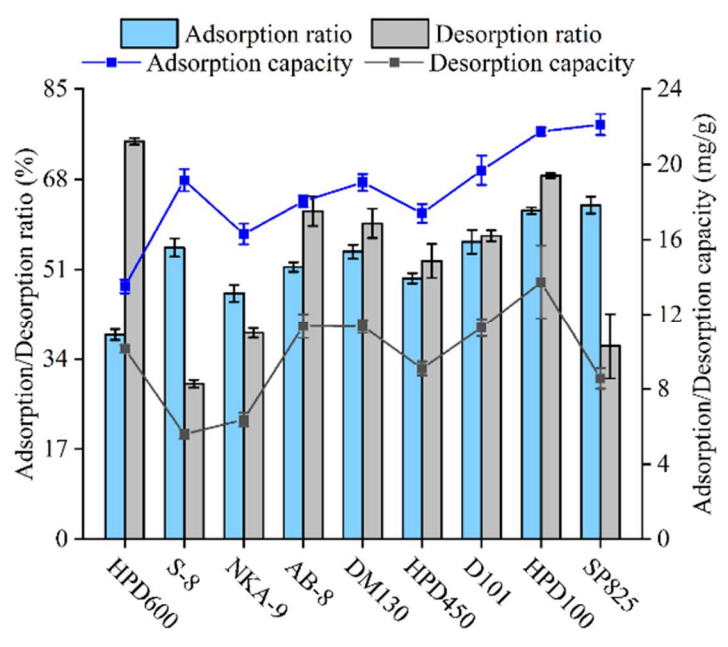


Fig. 1. LME adsorption and desorption capacities (mg/g) and ratios (%) across nine macroporous resins.

The adsorption capacity of macroporous resins for the target compound is influenced by the mass concentration of the sample solution, as shown in Fig. 2B. The adsorption capacity increases progressively with increasing concentration, reaching its peak at a concentration of 10 mg/ml. Beyond this point, further increases in concentration lead to a significant decline in the adsorption capacity. At lower sample concentrations, adsorption capacity exhibited a direct correlation with LME levels, driven by enhanced availability of active sites for target compound binding. Beyond this threshold, however, escalating LME promoted competitive adsorption of impurities onto the resin surface (Sun *et al.* 2013). This saturation effect led to a marginal decline in adsorption efficiency. Therefore, the concentration of LME selected for loading was 10 mg/ml.

Fig. 2C illustrates the effect of resin dosage on the adsorption of the target compound. As resin dosage increases, the adsorption efficiency of the target compound also rises. However, when the resin dosage reaches 7 g, further increases in dosage result in only marginal improvements in adsorption. To optimize resin use and minimize waste, a resin dosage of 7 g was selected as optimal.

As shown in Fig. 2D, the desorption capacity of the target compound increases progressively with the increasing volume fraction of the eluent. It reaches its maximum when the volume fraction reaches 60%. However, further increases in the volume fraction result in a decline in the desorption ratio. Based on these results, the desorption solvent concentration was optimized to 60% for subsequent experiments.

The effect of eluent volume on elution capacity is shown in the Fig. 2E. As the eluent volume increased from 20 to 30 ml, the desorption ratio of the resin continuously increased, reaching a maximum at 30 ml. Beyond this point, further increases in the eluent volume do not significantly change the desorption efficiency of the resin. Thus, the optimal purification performance is achieved with an eluent volume of 30 ml.

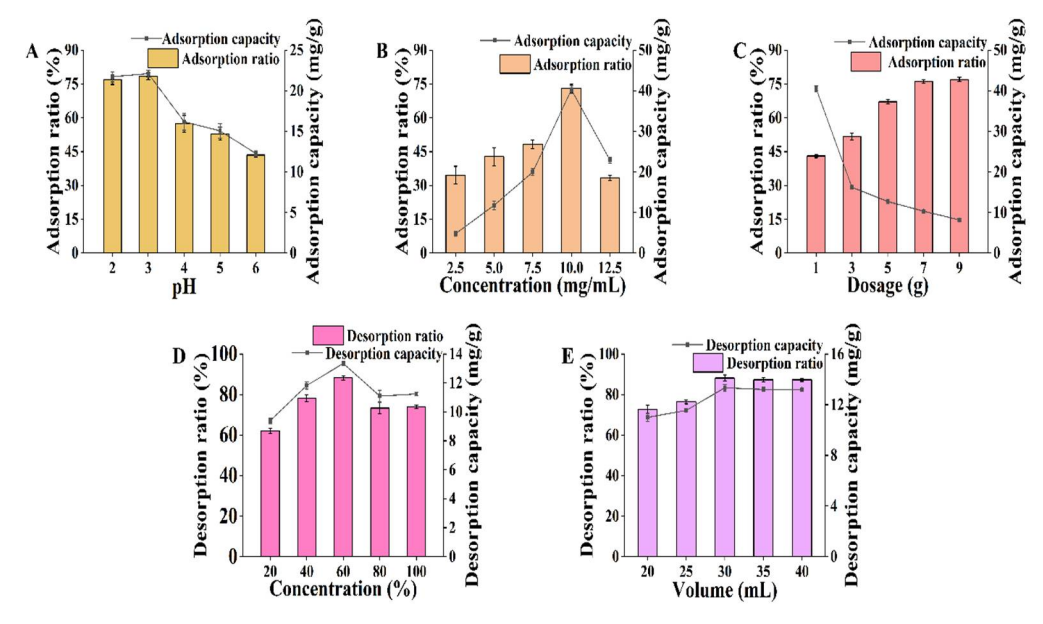


Fig. 2. Effects of the A: solution pH, B: solution concentration, C: resin dosage, D: eluent concentration, E: eluent volume on the purification efficiency of HPD100 Resin.

The dynamic leakage curve for HPD100 was constructed using the eluate volume and the concentration of the target compounds in the eluate. The leak point was defined as the volume at which the target compound's concentration in the eluate reached 10% of its concentration in the initial solution (Hou *et al.* 2019). An earlier leak point indicates lower adsorption efficiency of the macroporous resin. At a flow rate of 1.5 ml/min, the leak point occurred after approximately 200 ml of initial solution. At 2.0 ml/min, the leakage point was observed around 180 ml. Similarly, at a flow rate of 2.5 ml/min, the leak point was observed at approximately 180 ml (Fig. 3A). Therefore, a flow rate of 1.5 ml/min and a load volume of 200 ml were selected.

To further optimize the eluent flow velocity and eluent volume, dynamic elution curves were generated at different flow rates by monitoring the concentration of target compounds in the eluate over time. As shown in Fig 3B, the elution process was completed with approximately 300 ml of eluent at a flow rate of 1.5 ml/min. At 2 ml/min, complete elution required 220 ml of eluent, whereas at 2.5 ml/min, approximately 260 ml of eluent was needed for complete elution. Therefore, to maximize elution efficiency, an optimal flow rate of 2.0 ml/min was selected, with the corresponding eluent volume set at 220 ml.

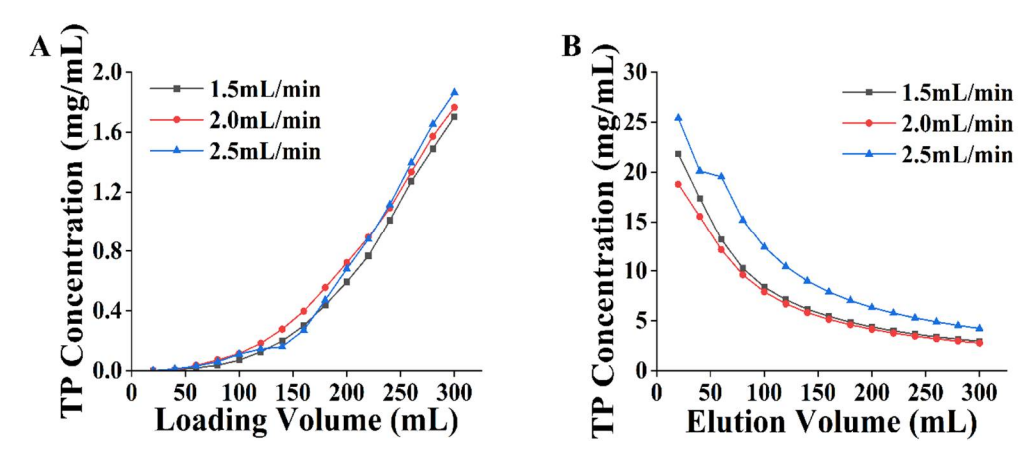


Fig. 3. Effects of the sample solution flow rate on the adsorption of HPD100 macroporous resin (A) and effect of the eluent flow rate on the desorption of HPD100 macroporous resin.

The TP content in the sample was determined as the sum of the contents of CA, NA, IAA, IAC. A calibration curve was generated by plotting the peak areas of standards against their concentrations. The standard curves were established as follows: for NA (y = 32950x - 744.54, $R^2 = 0.9996$), CA (y = 23411 x - 2903.7, $R^2 = 0.9997$), IAA (y = 56074 x - 1539, $R^2 = 0.9992$), IAC (y = 51638 x - 1617.8, $R^2 = 0.9995$).

The limits of detection (LODs) and limits of quantification (LOQs) for the four compounds ranged from 0.00836 to 0.12648 mg/ml and 0.02535 to 0.38328 mg/ml, respectively. The method validation for LME was also conducted. Intraday and interday precision were quantified through six replicate analyses conducted within a single day and across six consecutive days, respectively. Method validation showed intraday and interday relative standard deviations (RSDs) below 2%, confirming the method's high precision. The stability of the samples was tested at different time points under ambient conditions, with RSD values remaining below 2%, confirming the stability of the four compounds in the extract. Method repeatability was further verified by analyzing six identical samples, yielding RSD values below 2%, indicating good reproducibility. The recovery rates were determined by spiking LME with known amounts of the four standards. The results show that the established method achieved satisfactory recovery rates.

The adsorption kinetics were analyzed by monitoring the adsorption capacity at various time intervals. Initially, the adsorption capacity increased rapidly. At 40 min, the adsorption capacity rose more slowly, indicating the process was approaching saturation. Between 40 and 180 min, adsorption slowed as resins underwent autodesorption, with both processes occurring simultaneously (Hou *et al.* 2019) (Fig. 4A). The data were fitted to the pseudo-first-order, pseudo-second-order, and intra-particle diffusion kinetic models for further analysis. The fitting parameters revealed that the data did not align well with the pseudo-first-order and intra-particle diffusion models, which exhibited correlation coefficients (R^2) of 0.93575, 0.9999, 0.97888, 0.85406 and 0.96988, respectively. In contrast, the pseudo-second-order model provided the best fit, with an R^2 of 0.9999. The parameters obtained from this model were $k_2 = 0.01236$ and the calculated adsorption potential $q_e = 27.94857$ mg/g (Table 1), which closely matched the experimental value of 27.30451 mg/g. The pseudo-second-order model accurately describes the adsorption and purification of phenylpropanoids using HPD100 resin, indicating that the mechanism involves multilayer and complex adsorption interactions.

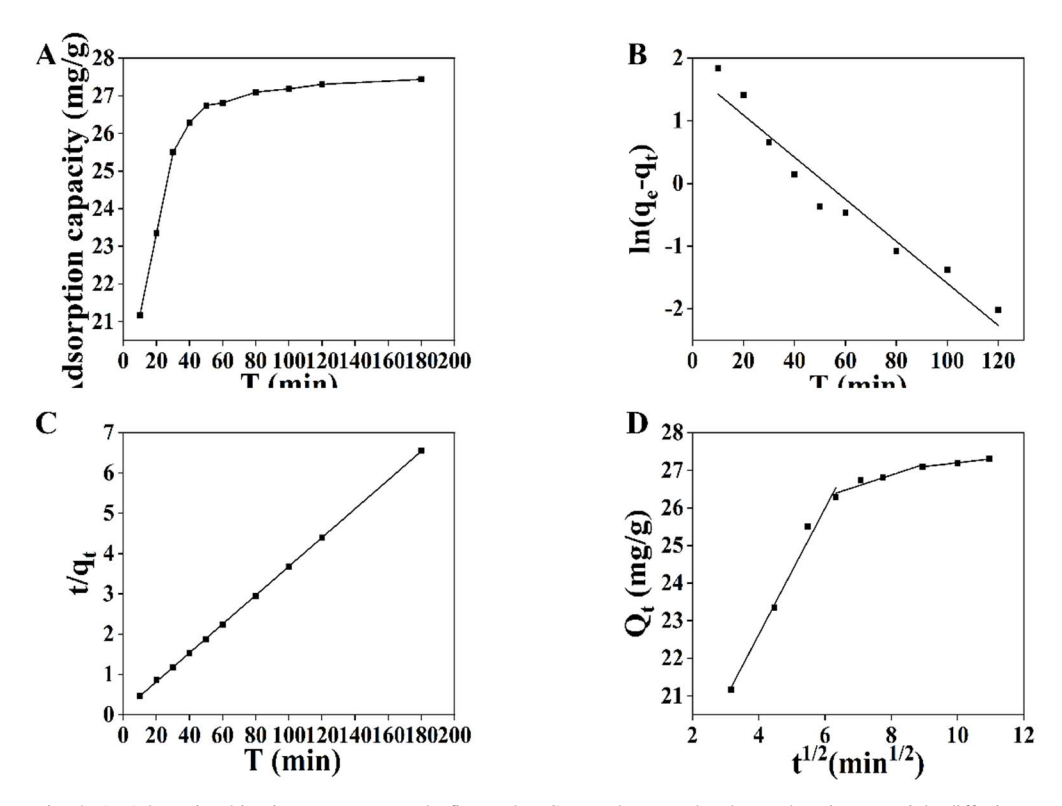


Fig. 4. A: Adsorption kinetic curve, B: pseudo-first-order, C: pseudo-second-order, and D: intra-particle diffusion models for purifying LME on the HPD100 resin.

Table 1. Kinetic model fitting equations and model parameters.

Dynamics Models	Kinetic Equations	Parameters
		$k_1 = 0.01458$
Pseudo-first-order model	ln(qe-qt) = -0.01458t + 0.76528	$R^2 = 0.93575$
		qe = 2.14960
		$k_2 = 0.01236$
Pseudo-second-order model	t/qt = 0.03578t + 0.10356	$R^2 = 0.9999$
		qe = 27.94857mg/g
		$k_p = 1.67997$
	$qt = 1.67997t^{1/2} + 15.90935$	$R^2 = 0.97888$
		C = 15.90935
	$qt = 0.2886t^{1/2} + 24.56336$	$k_p = 0.2886$
Intra-particle diffusion model		$R^2 = 0.85406$
•		C = 24.56336
		$k_p = 0.10236$
	$qt = 0.10236t^{1/2} + 26.17546$	$R^2 = 0.96988$
	-	C = 26.17546

As shown in Fig. 5A, adsorption capacity of HPD100 resin rose with initial phenylpropanoid concentration. Moreover, the inverse relationship with temperature indicates adsorption is favored at 25°C. Fig. 5B, C, D and Table 2 present the adsorption isotherm fitting results and parameters

for phenylpropanoids on resin at various temperatures. The Langmuir isotherm assumes a homogeneous monolayer of adsorption sites on the resin surface with no lateral interaction between adsorbed molecules. Moreover, increased Q_m values correspond to enhanced resin adsorption capacity (Chen et al. 2016). For phenylpropanoids on HPD100 resin, the maximum Q_m value was 155.29 mg/g at 35°C (Table 2). The positive correlation between Q_m and temperature suggests that the adsorption process is endothermic. The Freundlich model describes a heterogeneous resin surface with possible interactions between adjacent molecules. The K_F value, indicating adsorption capacity, decreases with increasing temperature, reinforcing the exothermic nature of the adsorption process. A 1/n ratio greater than 0.5 suggests that the resin's adsorption sites have varying energy levels, indicating complex interactions between the target molecules. This implies that sufficient resin or adsorption time is required to achieve the desired effect. In the Temkin model, K_T represents the binding affinity between the resin and the adsorbate. The results indicate that K_T decreases with increasing temperature, suggesting that higher temperatures weaken the interaction between the resin and phenylpropanoids. This implies that elevated temperatures are less favorable for the adsorption of phenylpropanoids. Compared to the Langmuir and Freundlich Temkin models, the Freundlich model, which showed a higher R², better explains the adsorption mechanism of phenylpropanoids on HPD100 resin.

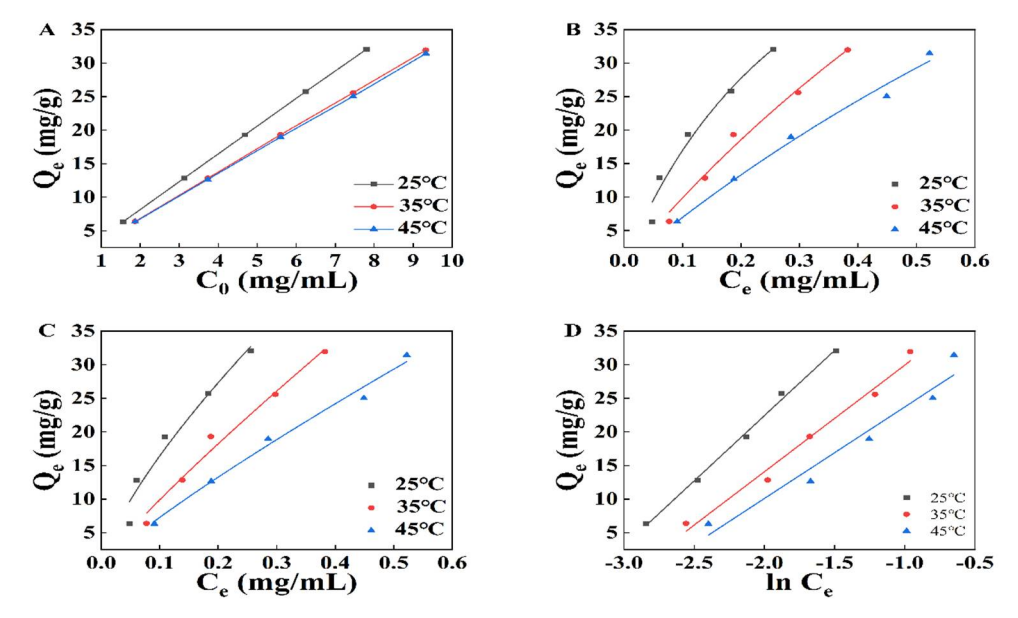


Fig. 5. The adsorption isotherms for LME on selected resin at different temperatures. A: Adsorption isotherms for LME on selected resin at 25 °C, 35 °C, and 45 °C. B: Langmuir adsorption isotherms for LME on selected resin. C: Freundlich adsorption isotherms for LME on HPD100 resin. D: Temkin isotherm adsorption isotherms for LME on HPD100 resin.

As shown in Table 3, the ΔH values indicate that the adsorption of the target compound by the resin is exothermic. The adsorption capacity decreases with increasing temperature, confirming that lower temperatures favor adsorption. Additionally, the absolute values of ΔH remain below the critical threshold of 40 kJ/mol, suggesting that the process is primarily governed by physical adsorption (Chen *et al.* 2016). This implies that the resin can be easily desorbed and regenerated. The negative ΔG values, presented in Table 3, confirm that the adsorption process is spontaneous

and irreversible. Furthermore, the absolute values of ΔG , all below 20 kJ/mol, further support the conclusion that the adsorption is primarily physical in nature (Zhong *et al.* 2019). A negative entropy change ($\Delta S < 0$) indicates a decrease in the degree of freedom during the adsorption process of target compounds, suggesting an entropy-reducing process (Limwachiranon *et al.* 2019). The thermodynamic parameters reveal that the adsorption of target compounds onto HPD100 resin is characterized by spontaneity, exothermicity, and a reduction in entropy, thus highlighting the preference for lower temperatures to facilitate this process.

Table 2. The adsorption isotherms and parameters of HPD100 resin towards LME at different temperatures.

Models	T(°C)	Equations	Parameters		
			K _L (ml/mg)	Q _m (mg/g)	\mathbb{R}^2
Langmuir	25	Ce/Qe = 0.01319Ce + 0.00458	2.87957	75.83213	0.95962
	35	Ce/Qe = 0.00644Ce + 0.00949	0.6783	155.29246	0.9813
	45	Ce/Qe = 0.00683Ce + 0.01366	0.50023	146.32082	0.98305
			$K_F [(mg/g)(ml/mg)^{1/n}]$	1/n	\mathbb{R}^2
Freundlich	25	lnQe = 0.73428lnCe + 4.48998	89.11966	0.73428	0.94647
	35	lnQe = 0.88203lnCe + 4.32297	75.412	0.88203	0.97665
	45	lnQe = 0.86592lnCe + 3.97916	53.47195	0.86592	0.98379
			K _T (ml/mg)	B _T (J/mol)	\mathbb{R}^2
Temkin	25	Qe = 19.40642lnCe + 61.24678	23.47674	19.40642	0.9949
	35	Qe = 15.85796lnCe + 45.79979	17.95969	15.85796	0.97732
	45	Qe = 13.64041 ln Ce + 37.37334	15.48544	13.64041	0.93604

Table 3. Adsorption thermodynamic of LME using HPD100 resin.

Qe(mg/g)	∆H(kJ/mol)	$\triangle G(kJ/mol)$				$\triangle S(kJ/mol)$	
	_	288K	298K	308K	288K	298K	308K
6.35532	-25.0934	-12.0896	-11.2984	-11.2249	-0.0436	-0.0448	-0.0436
19.3028	-38.6623	-12.8276	-11.8739	-11.0956	-0.0867	-0.0870	-0.0867
25.7612	-36.5137	-12.2592	-11.4045	-10.6323	-0.0814	-0.0815	-0.0814

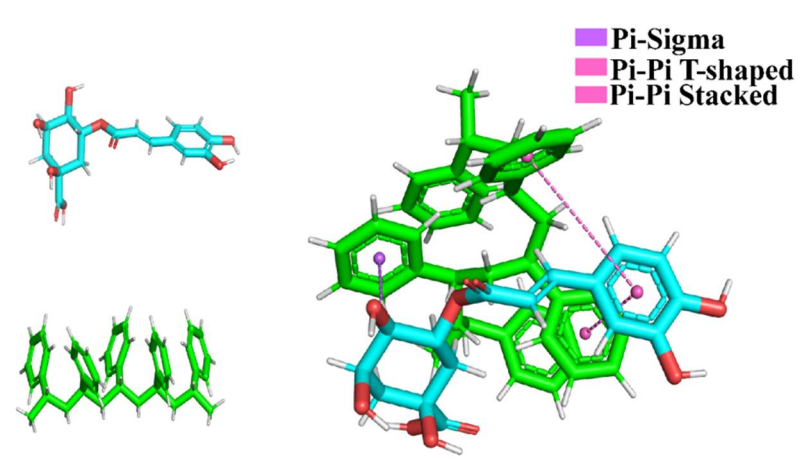


Fig. 6. Representation of molecular modeling, including: 3D structure of CA (left, top), 3D structure 32of polystyrene (left, bottom), 3D structure of the polymer interacting with CA (right).

Molecular docking simulations were performed using AutoDock Vina (version 1.2.0), with the molecular interactions visualized in Fig. 6 and the binding affinities quantitatively summarized in Table 4. As summarized in Table 4, the binding energy between chlorogenic acid and the resin is -3.388 kcal/mol. Further analysis revealed π - π and π - σ stacking interactions within the resinchlorogenic acid complex (Fig. 6). Overall, the docking results demonstrate that HPD100 resin possesses a strong binding affinity for chlorogenic acid, which is advantageous for the purification of the target compound.

Table 4. Binding energies of the two molecules from molecular docking.

Receptor	Ligand	Binding Energy
-	Polystyrene molecule / Chlorogenic acid molecule	-3.388

Nine macroporous resins were screened for TP purification from LME, with resin HPD100 proving most effective via HPLC. Optimal conditions were: 10 mg/ml LME, pH 3, 7 g resin, 60% eluent, 30 ml eluent volume, 1.5 ml/min load rate (200 ml total), and 2.0 ml/min elution rate (220 ml total). Adsorption followed a pseudo-second-order kinetic model and Freundlich isotherm; thermodynamics indicated spontaneous, exothermic adsorption. Molecular docking confirmed strong resin-compound binding.

Acknowledgements

This work was supported by the Science and Technology Program of Guizhou Province (Grant No. Qiankehe Zhicheng [2022] General 108) and the Science and Technology Program of Guizhou Province (Grant No. Qiankehe Zhicheng [2022] General 160).

References

- Alizadeh P, Alizadeh P, Rahimi M, Amjadi S, Bayati M and Nejad Ebrahimi S 2024. Enrichment of rosmarinic acid from comfrey (*Symphytum officinale* L.) root extract by macroporous adsorption resins and molecular docking studies. Ind. Crops Prod. **214**: 118541.
- Chen Y, Zhang W, Zhao T, Li F, Zhang M, Li J, Zou Y, Wang W, Cobbina SJ, Wu X and Yang L 2016. Adsorption properties of macroporous adsorbent resins for separation of anthocyanins from mulberry. Food Chem. **194**: 712-722.
- Dai C, Li H, Zhao W, Fu Y and Cheng J 2024. Bioactive functions of chlorogenic acid and its research progress in pig industry. J. Anim. Physiol. Anim. Nutr. 108(2): 439-450.
- He H, Zhang D, Gao J, Andersen TR and Mou Z 2019. Identification and evaluation of *Lonicera japonica* flos introduced to the Hailuogou area based on ITS sequences and active compounds. Peer J. 7: e7636.
- Hou M, Hu Wenzhong, Xiu Zhilong, Jiang A, Men L, Hao K, Sun X and Cao D 2019. Preparative Purification of Total Flavonoids from *Sophora tonkinensis* Gagnep. By Macroporous Resin Column Chromatography and Comparative Analysis of Flavonoid Profiles by HPLC-PAD. Molecules **24**: 3200.
- Hou M and Zhang L 2021. Adsorption/desorption characteristics and chromatographic purification of polyphenols from *Vernonia patula* (Dryand.) Merr. Using macroporous adsorption resin. Ind. Crops Prod. **170**: 113729.
- Li H, Hou G, Li Y, Zhao F, Cong W and Wang C 2018. Preparative separation of phloridzin from apple leaves using macroporous resins followed by preparative high-performance liquid chromatography. J. Sep. Sci. **41**(20): 3918-3924.
- Li Y, Liu Xiajin, Su Shulan, Yan H, Guo S, Qian D and Duan J 2022. Evaluation of Anti-Inflammatory and Antioxidant Effects of Chrysanthemum Stem and Leaf Extract on Zebrafish Inflammatory Bowel Disease Model. Molecules **27**(7): 2114.

- Limwachiranon J, Huang H, Li L, Duan Z and Luo Z 2019. Recovery of lotus (*Nelumbo nucifera* Gaertn.) seedpod flavonoids using polar macroporous resins: The updated understanding on adsorption/desorption mechanisms and the involved intermolecular attractions and bonding. Food Chem. **299**: 125108.
- Liu C, Li S, Gao Q, Qiao L, Li H, Yang S, Yan G, Lei J, Liang B, Kuang A, Zhang X, Wang G and Jiang Y 2024. Eco-friendly and efficient extraction of *Lonicera macranthoides* phenylpropanoid based on natural deep eutectic solvents: Process optimization, extraction mechanism and biological activity. Microchem. J. 198: 110133.
- Liu J, Zhang J, Wang F, Zou Y and Chen X 2013. Isolation and characterization of new minor triterpenoid saponins from the buds of *Lonicera macranthoides*. Carbohydr. Res. **370**: 76-81.
- Sun L, Guo Y, Fu C, Li J and Li Z 2013. Simultaneous separation and purification of total polyphenols, chlorogenic acid and phlorizin from thinned young apples. Food Chem. 136(2): 1022-1029.
- Sun Pengcheng, Liu Y, Yi Yuetao, Li Hongjuan, Fan P and Xia Chuanhai 2015. Preliminary enrichment and separation of chlorogenic acid from *Helianthus tuberosus* L. leaves extract by macroporous resins. Food Chem. **168**: 55-62.
- Wang XH and Wang JP 2023. Ultrasonic-assisted extraction and enrichment of the flavonoids from *Salicornia europaea* leaves using macroporous resins and response surface methodology. Chem. Pap. 77: 2769-2781.
- Zhong JL, Muhammad N, Gu YC and Yan WD 2019. A simple and efficient method for enrichment of cocoa polyphenols from cocoa bean husks with macroporous resins following a scale-up separation. J. Food Eng. **243**: 82-88.

(Manuscript received on 16 May 2025; revised on 11 October 2025)